20th Lomonosov Conference on Elementary Particle Physics

Examining axion-like particles with superconducting radio-frequency cavity

D. Kirpichnikov[1], D. Salnikov[1,2], P. Satunin[1], M. Fitkevich[1,3]

[1]Institute for Nuclear Research of the Russian Academy of Science
[2]Lomonosov Moscow State University
[3]Moscow Institute of Physics and Technology

25th of August, 2021

Traditional LSW-type experiments

- ALP Production: EM cavity mode + magnetic field → ALP
- ALP Detection: ALP + magnetic field → signal mode

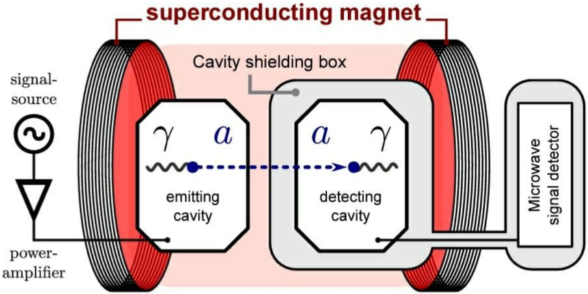

Figure 1 - The traditional LSW experiment scheme (CROWS)

The scheme of the proposed setup

- SRF cavities — larger quality factor and amplitudes for EM modes *but* external magnetic field destroys superconducting state (condition on the surface magnetic field: $|\vec{B}| < 0.2$ T for Niobium walls).
- In SRF cavities additional EM mode instead of magnetic field.

Z. Bogorad *et al.*, 2019;
R. Janish *et al.*, 2019;
C. Gao *et al.*, 2020.

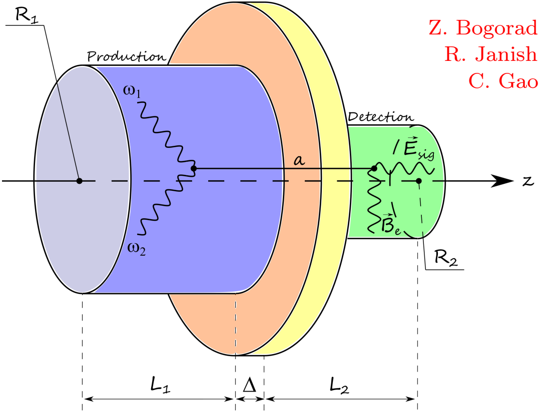

Figure 2 - The experiment scheme

Theoretical model

- Axion-like particles (ALPs) are described by massive real pseudo-scalar field of $a(\vec{x}, t)$ with mass of m_a.
- The Lagrangian ALPs - photon interaction:

$$\mathcal{L} = -\frac{1}{4} F_{\mu\nu} F^{\mu\nu} + \frac{1}{2} \partial_\mu a \, \partial^\mu a - \frac{1}{2} m_a^2 a^2 + \frac{g_{a\gamma\gamma}}{4} \, a \, F_{\mu\nu} \tilde{F}^{\mu\nu} \; , \qquad (1)$$

where $g_{a\gamma\gamma}$ - coupling constant, $\tilde{F}^{\mu\nu} = \frac{1}{2} \varepsilon^{\mu\nu\alpha\beta} F_{\alpha\beta}$ - dual field tensor.

- The Lagrangian (1) yields the following equations of motion:

$$(\partial_\mu \partial^\mu + m_a^2) \, a = \frac{g_{a\gamma\gamma}}{4} F_{\mu\nu} \tilde{F}^{\mu\nu}, \qquad (2)$$

$$\partial_\mu F^{\mu\nu} = g_{a\gamma\gamma} \, \tilde{F}^{\mu\nu} \partial_\mu a. \qquad (3)$$

Production of axion-like particles

- If the electromagnetic invariant

$$F_{\mu\nu}\tilde{F}^{\mu\nu} = -4(\vec{E}\cdot\vec{B}) \tag{4}$$

  is non-vanishing then Eq. (2) implies that the axion field can be produced.
- For a single TM_{npq} or TE_{npq} mode $(\vec{E}\cdot\vec{B}) = 0$. Thus it is necessary to use at least two modes.
- In this case two axion waves are produced:

$$a_{\pm}(\vec{x},t) = -\frac{g_{a\gamma\gamma}}{4\pi}\Re\mathrm{e}\int\limits_{V_{cav}} \mathrm{d}^3x' \, \frac{F_{\pm}(\vec{x}')}{|\vec{x}-\vec{x}'|}\cdot \mathrm{e}^{ik_{\pm}|\vec{x}-\vec{x}'|-i\omega_{\pm}t}, \tag{5}$$

where $k_{\pm} = \sqrt{\omega_{\pm}^2 - m_a^2}$, $\omega_{\pm} = |\omega_1 \pm \omega_2|$, $\omega_{1,2}$ - frequencies of pump modes, $F_{\pm}(\vec{x})$ - functions of their complex amplitudes.

Modelling of axion field

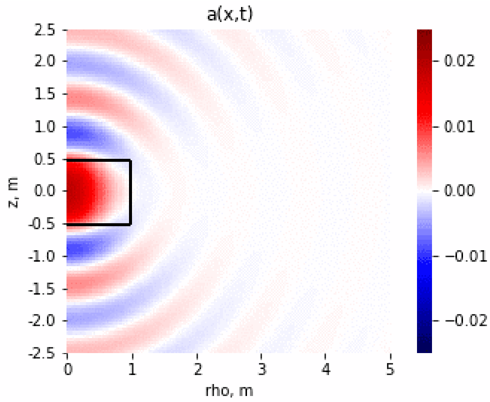

$$m = 8 \cdot 10^{-7} \text{ eV},$$

$$R_1 = 1 \text{ m}, \ L_1 = 1 \text{ m}, \ \omega_+ = 14.7 \cdot 10^{-7} \text{ eV}.$$

Time-averaged energy density of ALPs

- To describe the intensity of ALPs production, the time-average energy density was calculated:

$$\langle \rho^E_\pm \rangle_T = \frac{1}{2}\langle \dot{a}^2_\pm \rangle_T + \frac{1}{2}\langle \partial_i a_\pm \partial^i a_\pm \rangle_T + \frac{1}{2} m_a^2 \langle a^2_\pm \rangle_T \ . \tag{6}$$

- The spatial distribution of the time-average energy density (6) depends on:
  - mass of ALPs;
  - cylindrical cavity geometry;
  - pump modes.

Comparison of $\langle \rho_+^E \rangle$ and $\langle \rho_-^E \rangle$

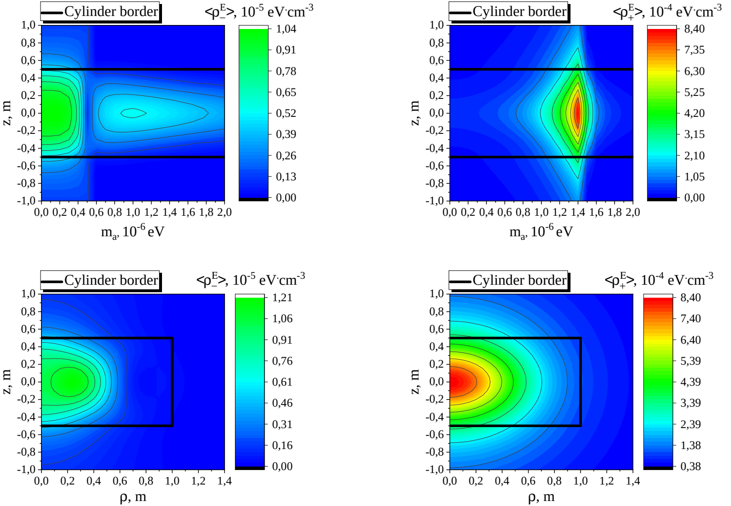

Figure 3 - The time-averaged energy density of ALPs for $TM_{010} + TE_{011}$ pump modes

Comparison of various combinations of pump modes

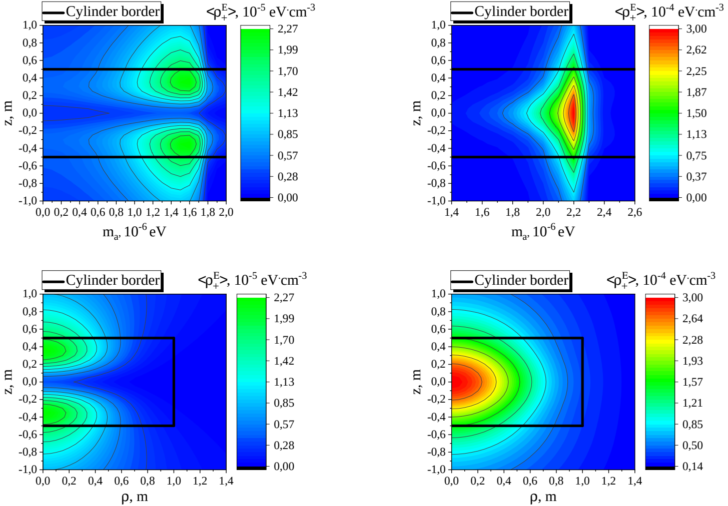

Figure 4 - The time-averaged energy density of ALPs for $TM_{011} + TE_{011}$ and $TM_{011} + TE_{012}$ pump modes

Comparison of various geometry of cavity

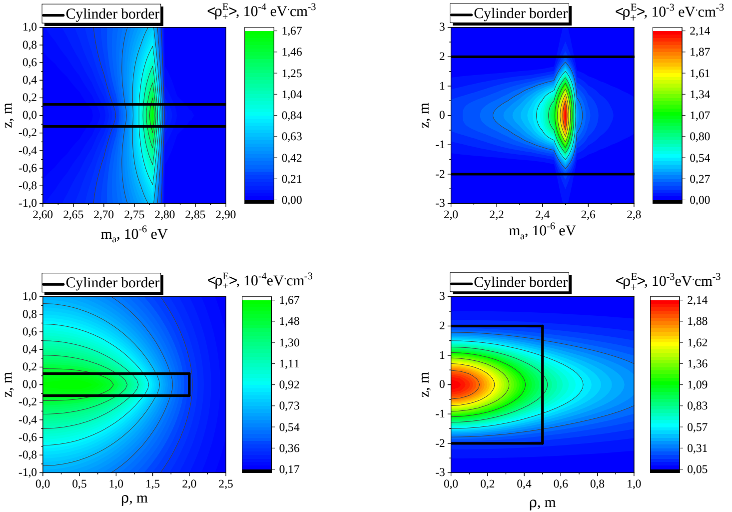

Figure 5 - The time-averaged energy density of ALPs for TM_{010} + TE_{011} pump modes for various cavity geometry

Radiation pattern

- Consider the expression (5) for $a_\pm(\vec{x},t)$:

$$a_\pm(\vec{x},t) = -\frac{g_{a\gamma\gamma}}{4\pi}\Re\mathrm{e} \int\limits_{V_{cav}} \mathrm{d}^3x' \, \frac{F_\pm(\vec{x}')}{|\vec{x}-\vec{x}'|} \cdot \mathrm{e}^{ik_\pm|\vec{x}-\vec{x}'|-i\omega_\pm t}. \tag{5}$$

- In far distance where $|\vec{x}| \gg |\vec{x}'|$ let us decompose integrand in the formula (5) by a small parameter $\vec{x}'$. Then we obtain the asymptotic formula:

$$a_\pm(\vec{x},t) = -\frac{g_{a\gamma\gamma}}{4\pi|\vec{x}|}\Re\mathrm{e}\, \mathrm{e}^{ik_\pm|\vec{x}|-i\omega_\pm t} \int\limits_{V_{cav}} \mathrm{d}^3\vec{x}' \; F_\pm(\vec{x}')\cdot\exp\left[-ik_\pm\left(\vec{x}'\cdot\frac{\vec{x}}{|\vec{x}|}\right)\right] + o\left(\frac{1}{|\vec{x}|}\right). \tag{7}$$

- Definition of the function of radiation pattern:

$$f_\pm(\varphi,\theta) = \lim_{|\vec{x}|\to\infty} \frac{\langle a_\pm^2\rangle_T}{\max\limits_{\varphi,\theta}\langle a_\pm^2\rangle_T}. \tag{8}$$

Radiation pattern

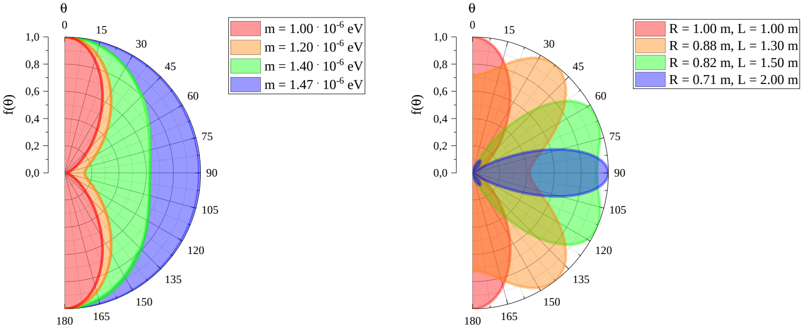

Figure 6 - Radiation pattern for $TM_{010} + TE_{011}$ pump modes for various masses of ALPs and cylindrical cavity geometries

ALPs detection

- The equation (3)

$$\partial_\mu F^{\mu\nu} = g_{a\gamma\gamma}\, \tilde{F}^{\mu\nu} \partial_\mu a. \tag{3}$$

  describes the generation of a signal electromagnetic field during the interaction of ALPs with the field $\vec{B}_e$.

- The decomposition of the signal electromagnetic field by the eigenmodes of the *detection* cavity is considered:

$$\vec{E}^{\rm sig}(\vec{x}, t) = \sum_m \vec{\mathcal{E}}_m(\vec{x}) E_m^{\rm sig}(t)\ . \tag{9}$$

- The number of produced photons of the signal mode can be estimated according to the following relation:

$$N_s \simeq \frac{1}{2\omega} \int\limits_{2\,\rm cav} \mathrm{d}^3 x \, \langle |\vec{E}^{\rm sig}(\vec{x}, t)|^2 \rangle \simeq \frac{V_2}{2\omega} \langle |E_m^{\rm sig}(t)|^2 \rangle\ . \tag{10}$$

ALPs detection

- The average energy density of the signal mode is expressed with the following equation:

$$\langle |E_m^{\mathrm{sig}}(t)|^2 \rangle = \frac{1}{2}\left[\frac{g_{a\gamma\gamma}^2 E_0^2 Q B_c^z}{4\pi} \cdot \frac{V_{1\,\mathrm{cav}}}{\Delta} \cdot \kappa_m^{\pm}\right]^2 . \tag{11}$$

- Signal-to-noise ratio:

$$\mathrm{SNR} \simeq \frac{N_s}{N_{\mathrm{th}}} \frac{1}{2 L_2 Q} \sqrt{\frac{t}{B}} . \tag{12}$$

- Finally, we obtain the estimate of coupling constant at which ALPs can be detected by considered experimental model:

$$g_{a\gamma\gamma} \simeq \left[\frac{128\pi^2 T L_2 \Delta^2}{E_0^4 (B_c^z)^2 Q \kappa_m^2 V_1^2 V_2} \sqrt{\frac{B}{t}} \mathrm{SNR}\right]^{1/4} . \tag{13}$$

Experimental model sensitivity

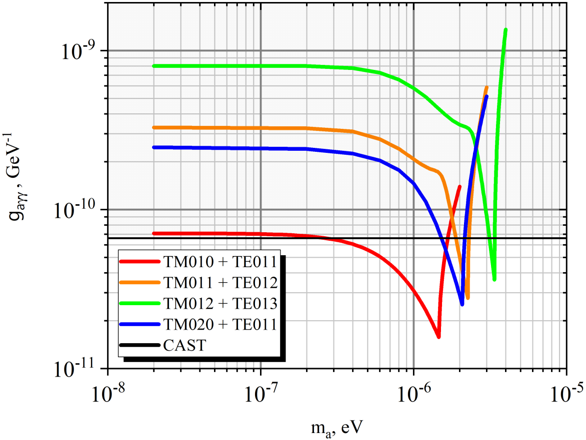

Figure 7 - Dependence of the coupling constant $g_{a\gamma\gamma}$ on the mass of ALPs m_a for various pump modes of the *production* cavity ($R_1 = 1$ m, $L_1 = 1$ m) for the TM_{010} mode of the *detecting* cavity

Conclusions

- The time-average energy density $\langle\rho_+^E\rangle_T$ dominates over the time-average energy density $\langle\rho_-^E\rangle_T$;
- The time-average energy density $\langle\rho_+^E\rangle_T$ has a «resonance» at ALPs with the mass of $m_a \lesssim \omega_+$;
- The spacial distribution of the time-average energy density $\langle\rho_+^E\rangle_T$ significantly depends on pump modes. The most optimal ones are modes satisfied following relation: $n_1 = n_2$ and odd $q_1 + q_2$;
- The radiation pattern of ALPs depends on cavity geometry and their momentum. The conditions under which a particular type of radiation pattern is realized are considered;
- The experimental model sensitivity corresponds to other experiments. The most optimal pump modes for lower mass of ALPs m_a of production cavity are TM_{010}+TE_{011}.

References

- More detailed results are posted in the article:

  D. Salnikov, P. Satunin, D. Kirpichnikov, M. Fitkevich, «Examining axion-like particles with superconducting radio-frequency cavity». J. High Energ. Phys. 2021, **143** (2021). doi:10.1007/JHEP03(2021)143 [arXiv:2011.12871 [hep-ph]];

- The program code is posted on the website: https://github.com/dmitry-salnikov-msu/Axion;

- For acceleration, parallel calculations were applied using the MPI software interface. The calculations were carried out on the INR RAS cluster: http://cluster.inr.ac.ru/for_users.php.

Further research

- Further plans include the following research:
  - analysis of another configuration of the experimental model, in which the generating cavity has the shape of a «tube», and the detecting cavity is a cylindrical layer around it:

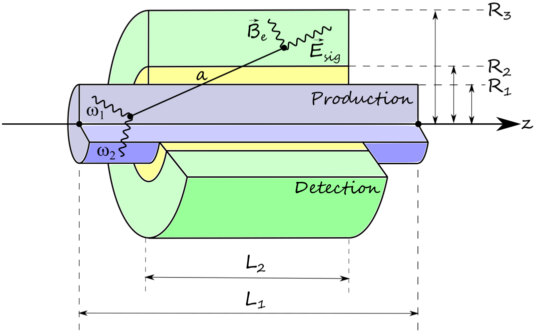

Figure 8 - Projected design of the experimental setup

Further research

- optimization of the experiment: selection of the most suitable geometry of the generating and detecting cavities, their relative positions and the mode of generation of ALPs (ultra-relativistic or non-relativistic);
- description of the interaction of ALPs with the field $\vec{B}_e$ in the detecting cavity in the QFT terms to obtain more accurate results;
- a study of another type of experiment in which the production and detection of ALPs occurs in a single cavity.

Thank you for attention!

Source function

- The expressions for the electromagnetic field have the form:

$$\vec{E}_i(\vec{x},t) = \sqrt{2}\Re\mathrm{e}\left[\vec{\mathcal{E}}_i(\vec{x},\omega_i)e^{-i\omega_i t}\right],\ i=1,2; \tag{14}$$

$$\vec{B}_i(\vec{x},t) = \sqrt{2}\Re\mathrm{e}\left[\vec{\mathcal{B}}_i(\vec{x},\omega_i)e^{-i\omega_i t}\right],\ i=1,2; \tag{15}$$

where $\vec{\mathcal{E}}_i(\vec{x},\omega_i)$ and $\vec{\mathcal{B}}_i(\vec{x},\omega_i)$ - complex amplitudes of TM_{npq} and TE_{npq} pump modes

- For the scalar product $(\vec{E}\cdot\vec{B})$ we obtain:

$$\left(\vec{E}(\vec{x},t)\cdot\vec{B}(\vec{x},t)\right) = \Re\mathrm{e}\left[F_+(\vec{x})\cdot\mathrm{e}^{-i\omega_+ t} + F_-(\vec{x})\cdot\mathrm{e}^{-i\omega_- t}\right]\ , \tag{16}$$

where $\omega_\pm = |\omega_1 \pm \omega_2|$,

$$F_+(\vec{x}) \equiv \vec{\mathcal{E}}_1(\vec{x})\cdot\vec{\mathcal{B}}_2(\vec{x}) + \vec{\mathcal{E}}_2(\vec{x})\cdot\vec{\mathcal{B}}_1(\vec{x})\ , \tag{17}$$

$$F_-(\vec{x}) \equiv \vec{\mathcal{E}}_1^*(\vec{x})\cdot\vec{\mathcal{B}}_2(\vec{x}) + \vec{\mathcal{E}}_2(\vec{x})\cdot\vec{\mathcal{B}}_1^*(\vec{x})\ . \tag{18}$$

Exact form of TM$_{npq}$ modes

- TM$_{npq}$ modes are expressed in terms of the electric and magnetic fields as:

$$\mathcal{E}_z^{TMnpq} = \mathcal{E}_0 J_n\left(\frac{x_{np}}{R}\rho\right)\left\{\begin{array}{c}\sin n\varphi\\ \cos n\varphi\end{array}\right\}\cos\left(\frac{q\pi}{L}z\right),$$

$$\mathcal{E}_\rho^{TMnpq} = \frac{-\mathcal{E}_0}{k_{npq}^2-(q\pi/L)^2}\cdot\frac{q\pi}{L}\cdot\frac{x_{np}}{R}\cdot J_n'\left(\frac{x_{np}}{R}\rho\right)\left\{\begin{array}{c}\sin n\varphi\\ \cos n\varphi\end{array}\right\}\sin\left(\frac{q\pi}{L}z\right),$$

$$\mathcal{E}_\varphi^{TMnpq} = \frac{-\mathcal{E}_0}{k_{npq}^2-(q\pi/L)^2}\cdot\frac{1}{\rho}\cdot\frac{nq\pi}{L}\cdot J_n\left(\frac{x_{np}}{R}\rho\right)\left\{\begin{array}{c}\cos n\varphi\\ -\sin n\varphi\end{array}\right\}\sin\left(\frac{q\pi}{L}z\right),$$

$$\mathcal{B}_z^{TMnpq} = 0,$$

$$\mathcal{B}_\rho^{TMnpq} = \frac{-i\omega_{npq}^{TM}\mathcal{E}_0}{k_{npq}^2-(q\pi/L)^2}\cdot\frac{n}{\rho}\cdot J_n\left(\frac{x_{np}}{R}\rho\right)\left\{\begin{array}{c}\cos n\varphi\\ -\sin n\varphi\end{array}\right\}\cos\left(\frac{q\pi}{L}z\right),$$

$$\mathcal{B}_\varphi^{TMnpq} = \frac{i\omega_{npq}^{TM}\mathcal{E}_0}{k_{npq}^2-(q\pi/L)^2}\cdot\frac{x_{np}}{R}\cdot J_n'\left(\frac{x_{np}}{R}\rho\right)\left\{\begin{array}{c}\sin n\varphi\\ \cos n\varphi\end{array}\right\}\cos\left(\frac{q\pi}{L}z\right);$$

Exact form of TE$_{npq}$ modes

- TE$_{npq}$ modes are expressed in terms of the electric and magnetic fields as:

$$\mathcal{B}_z^{TEnpq} = \mathcal{B}_0 J_n\left(\frac{x'_{np}}{R}\rho\right)\left\{\begin{array}{c}\sin n\varphi\\ \cos n\varphi\end{array}\right\}\sin\left(\frac{q\pi}{L}z\right),$$

$$\mathcal{B}_\rho^{TEnpq} = \frac{\mathcal{B}_0}{k_{npq}^2-(q\pi/L)^2}\cdot\frac{q\pi}{L}\cdot\frac{x'_{np}}{R}\cdot J'_n\left(\frac{x'_{np}}{R}\rho\right)\left\{\begin{array}{c}\sin n\varphi\\ \cos n\varphi\end{array}\right\}\cos\left(\frac{q\pi}{L}z\right),$$

$$\mathcal{B}_\varphi^{TEnpq} = \frac{\mathcal{B}_0}{k_{npq}^2-(q\pi/L)^2}\cdot\frac{1}{\rho}\cdot\frac{nq\pi}{L}\cdot J_n\left(\frac{x'_{np}}{R}\rho\right)\left\{\begin{array}{c}\cos n\varphi\\ -\sin n\varphi\end{array}\right\}\cos\left(\frac{q\pi}{L}z\right),$$

$$\mathcal{E}_z^{TEnpq} = 0,$$

$$\mathcal{E}_\rho^{TEnpq} = \frac{i\omega_{npq}^{TE}\mathcal{B}_0}{k_{npq}^2-(q\pi/L)^2}\cdot\frac{n}{\rho}\cdot J_n\left(\frac{x'_{np}}{R}\rho\right)\left\{\begin{array}{c}\cos n\varphi\\ -\sin n\varphi\end{array}\right\}\sin\left(\frac{q\pi}{L}z\right),$$

$$\mathcal{E}_\varphi^{TEnpq} = \frac{-i\omega_{npq}^{TE}\mathcal{B}_0}{k_{npq}^2-(q\pi/L)^2}\cdot\frac{x'_{np}}{R}\cdot J'_n\left(\frac{x'_{np}}{R}\rho\right)\left\{\begin{array}{c}\sin n\varphi\\ \cos n\varphi\end{array}\right\}\sin\left(\frac{q\pi}{L}z\right).$$

Geometrical form-factor of $\kappa_m^{\pm}$

- Recall the expression for the time-average energy density of the signal electromagnetic mode:

$$\langle |E_m^{\mathrm{sig}}(t)|^2 \rangle = \frac{1}{2}\left[\frac{g_{a\gamma\gamma}^2 E_0^2 Q B_c^z}{4\pi} \cdot \frac{V_{1\,\mathrm{cav}}}{\Delta} \cdot \kappa_m^{\pm}\right]^2 . \tag{11}$$

- The geometrical form-factor of $\kappa_m^{\pm}$ is

$$\kappa_m^{\pm} = \sqrt{(\kappa_{m\,\mathrm{cos}}^{\pm})^2 + (\kappa_{m\,\mathrm{sin}}^{\pm})^2}, \tag{19}$$

where

$$\kappa_{m\,\mathrm{sin}}^{\pm\,\mathrm{cos}} = \left(\alpha_{m\,\mathrm{sin}}^{\pm\,\mathrm{cos}} + \frac{\beta_{m\,\mathrm{sin}}^{\pm\,\mathrm{cos}}}{\omega_{\pm}^2 L_1^2}\right) . \tag{20}$$

Geometrical form-factor of $\kappa_m^{\pm}$

- The geometrical form-factors of $\alpha^{\pm\,\cos}_{m\,\sin}$ and $\beta^{\pm\,\cos}_{m\,\sin}$ have the form:

$$\alpha^{\pm\,\cos}_{m\,\sin} = \int\limits_{2\,\mathrm{cav}} \frac{d^3x}{V_2}\,\mathcal{E}^z_m(\vec{x}) \int\limits_{1\,\mathrm{cav}} \frac{d^3x'}{V_1}\frac{|F_\pm(\vec{x}\,')|}{E_0^2}\cdot\frac{\Delta}{|\vec{x}-\vec{x}'|}\left\{\begin{array}{c}\cos\left(k_\pm|\vec{x}-\vec{x}'|\right)\\ \sin\left(k_\pm|\vec{x}-\vec{x}'|\right)\end{array}\right\},$$

$$\beta^{\pm\,\cos}_{m\,\sin} = \int\limits_{2\,\mathrm{cav}} \frac{d^3x}{V_2}\,\mathcal{E}^z_m(\vec{x}) \int\limits_{1\,\mathrm{cav}} \frac{d^3x'}{V_1}\frac{\partial^2_{z'}\,|F_\pm(\vec{x}\,')|}{E_0^2}\cdot\frac{\Delta\cdot L_1^2}{|\vec{x}-\vec{x}'|}\left\{\begin{array}{c}\cos\left(k_\pm|\vec{x}-\vec{x}'|\right)\\ \sin\left(k_\pm|\vec{x}-\vec{x}'|\right)\end{array}\right\} -$$

$$- \int\limits_{2\,\mathrm{cav}} \frac{d^3x}{V_2}\,\mathcal{E}^z_m(\vec{x}) \int\limits_{1\,\mathrm{S}} \frac{\rho'\,d\rho'\,d\varphi'}{V_1}\frac{\partial_{z'}|F_\pm(\vec{x}')|}{E_0^2}\cdot\frac{\Delta\cdot L_1^2}{|\vec{x}-\vec{x}'|}\left\{\begin{array}{c}\cos\left(k_\pm|\vec{x}-\vec{x}'|\right)\\ \sin\left(k_\pm|\vec{x}-\vec{x}'|\right)\end{array}\right\}\Bigg|_{z'=0}^{z'=L}.$$

Modelling of axion field

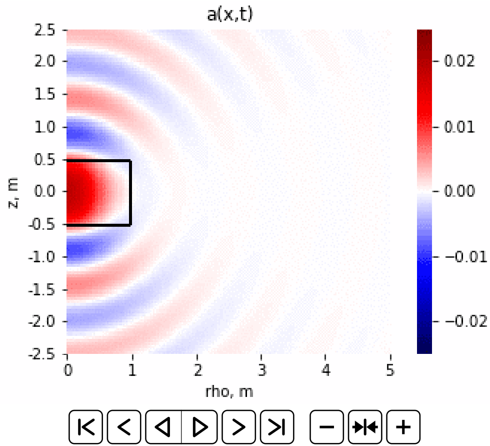

$$m = 8 \cdot 10^{-7} \text{ eV},$$

$$R_1 = 1 \text{ m}, \ L_1 = 1 \text{ m}, \ \omega_+ = 14.7 \cdot 10^{-7} \text{ eV}.$$

Modelling of axion field

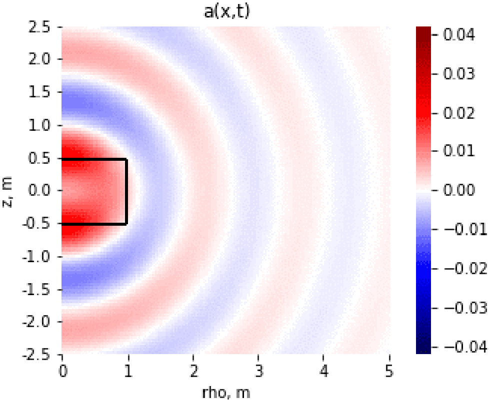

$$m = 12 \cdot 10^{-7}\ \text{eV},$$

$$R_1 = 1\ \text{m},\ \ L_1 = 1\ \text{m},\ \ \omega_+ = 14.7 \cdot 10^{-7}\ \text{eV}.$$

Modelling of axion field

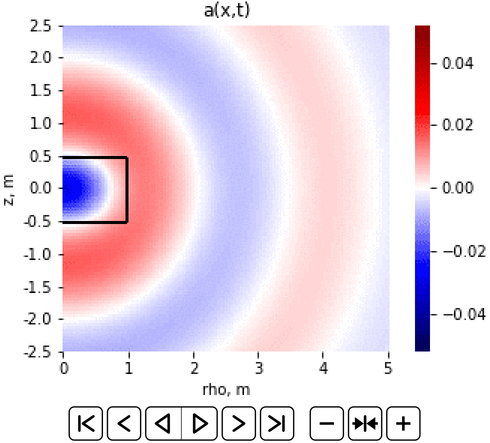

$$m = 14 \cdot 10^{-7} \text{ eV},$$

$$R_1 = 1 \text{ m}, \; L_1 = 1 \text{ m}, \; \omega_+ = 14.7 \cdot 10^{-7} \text{ eV}.$$

Modelling of axion field

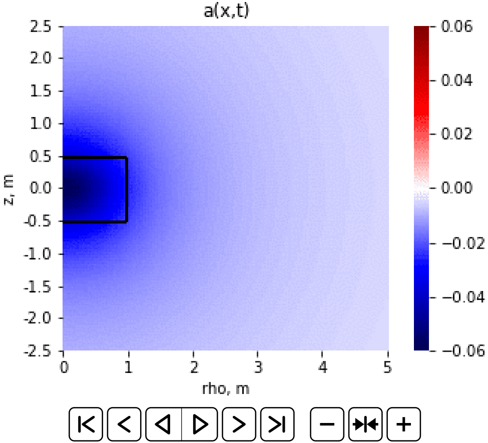

$$m = 14.7 \cdot 10^{-7}\ \text{eV},$$

$$R_1 = 1\ \text{m},\ L_1 = 1\ \text{m},\ \omega_+ = 14.7 \cdot 10^{-7}\ \text{eV}.$$

Modelling of axion field

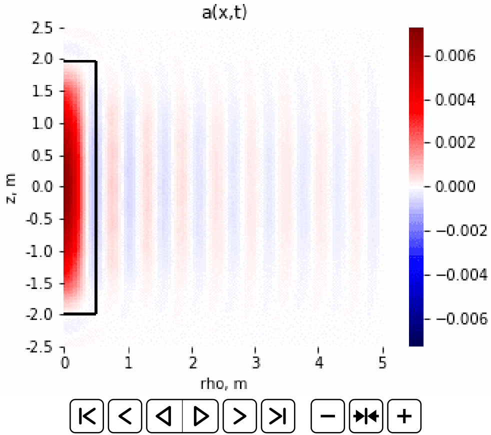

$$m = 10 \cdot 10^{-7} \text{ eV},$$

$$R_1 = 0.5 \text{ m}, \;\; L_1 = 4 \text{ m}, \;\; \omega_+ = 25.0 \cdot 10^{-7} \text{ eV}.$$

Modelling of axion field

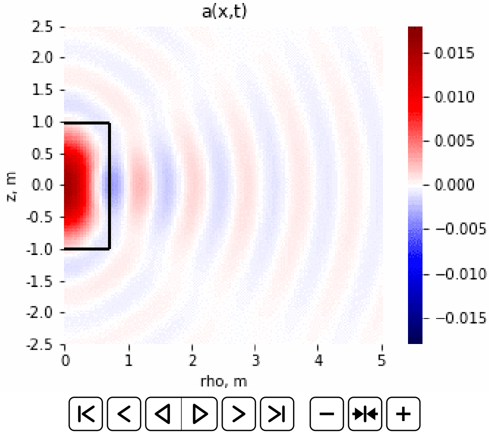

$$m = 10 \cdot 10^{-7} \text{ eV},$$

$$R_1 = 0.71 \text{ m}, \;\; L_1 = 2 \text{ m}, \;\; \omega_+ = 18.0 \cdot 10^{-7} \text{ eV}.$$

Modelling of axion field

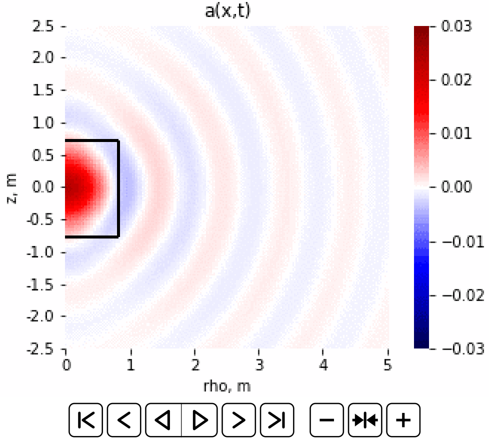

$$m = 10 \cdot 10^{-7} \text{ eV},$$

$$R_1 = 0.82 \text{ m}, \;\; L_1 = 1.5 \text{ m}, \;\; \omega_+ = 16.1 \cdot 10^{-7} \text{ eV}.$$

Modelling of axion field

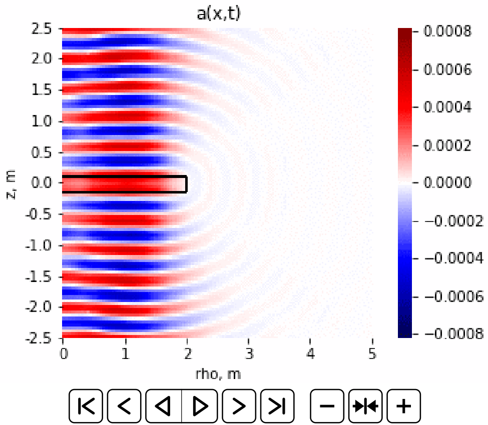

$$m = 10 \cdot 10^{-7} \text{ eV},$$

$$R_1 = 2 \text{ m}, \; L_1 = 0.25 \text{ m}, \; \omega_+ = 27.8 \cdot 10^{-7} \text{ eV}.$$